JOURNAL OF SOLID STATE CHEMISTRY **135,** 86–95 (1998)
ARTICLE NO. SC977600

Calcium–Lead Hydroxyapatites: Thermal and Structural Properties and the Oxidation of Methane

Shigeru Sugiyama,*,[1] Toshimitsu Minami,* Toshihiro Moriga,* Hiromu Hayashi,* and John B. Moffat†

*Department of Chemical Science and Technology, Faculty of Engineering, The University of Tokushima, Minamijosanjima, Tokushima 770, Japan; and †Department of Chemistry and the Guelph–Waterloo Centre for Graduate Work in Chemistry, University of Waterloo, Waterloo, Ontario N2L 3G1, Canada

Received March 17, 1997; in revised form August 12, 1997; accepted August 21, 1997

The oxidation of methane on calcium (HAp) and calcium–lead hydroxyapatites (PbHAp) has been studied in the presence and absence of tetrachloromethane (TCM) as a gas-phase additive. In the absence of TCM both the conversion and selectivities were strongly influenced by the structure and/or the lead content of the catalysts, particularly at 973 K. The addition of lead produced substantial increases the C_{2+} selectivities with concomitant decreases in that of the carbon oxides while the introduction of TCM suppressed the formation of CO_2, apparently resulting from the formation of chlorapatites. Significant differences between the results observed at reaction temperatures of 873 and 973 K can be attributed to the structural transformation of the hydroxyapatites to the corresponding phosphates at the higher temperature. Extended X-ray absorption fine structure spectroscopy has been employed to provide further information on the relevant structural factors in the oxidation process. © 1998 Academic Press

INTRODUCTION

Calcium hydroxyapatites $[Ca_{10-x}(HPO_4)_x(PO_4)_{6-x}(OH)_{2-x}, O \leq x \leq 1]$ are bifunctional catalysts with acidic and basic properties which are dependent upon their compositions (1–7). The stoichiometric form ($x = 0$) has been shown to possess basic sites, while the nonstoichiometric forms function as acids. Calcium may be replaced by other cations such as lead while the crystallographic structure is retained although, not surprisingly, substitution of the latter species results in an increase in the size of the unit cell (8–11).

Although solids containing lead have been shown to be catalytically active in the oxidative coupling of methane to produce C_2 hydrocarbons, the high volatility of lead is a detriment to their stabilities (12–35). In contrast, the hydroxyapatites where lead has been introduced are relatively stable and have been shown to catalyze the selective coupling of methane (36–38) unlike with calcium and strontium hydroxyapatites with which the principal products are carbon oxides (39–46).

Earlier work from our laboratories has shown that the introduction of small partial pressures of tetrachloromethane (TCM) to the feedstream for the conversion of methane generally produces advantageous effects (47). Thus, for example, in the oxidative coupling of methane the conversion and the selectivity to C_{2+} hydrocarbons have been observed to increase while recent results reveal increased selectivities to carbon monoxide in the partial oxidation of methane on stoichiometric and nonstoichiometric calcium (41–43, 47) and strontium (45–47) hydroxyapatites. In contrast, with strontium hydroxyapatites ion-exchanged with lead, methyl chloride with selectivities as high as 70% was obtained with TCM in the feedstream (48, 49). The effects of the addition of TCM have tentatively been attributed to the formation of chlorapatites resulting from the exchange of hydroxyl groups by chlorine in the hydroxyapatites (41–43, 45, 46, 48, 49).

The thermal and catalytic properties of calcium and calcium–lead hydroxyapatites in the oxidation of methane with and without TCM as a gas-phase additive are described in the present report. The catalysts have been characterized by X-ray diffraction (XRD), X-ray photoelectron spectroscopy (XPS), and extended X-ray absorption fine structure spectroscopy (EXAFS).

EXPERIMENTAL

Catalyst Preparation

Calcium and lead–calcium hydroxyapatites were prepared from $Na_2HPO_4 \cdot 12H_2O$ (Wako Pure Chemicals, Osaka), $Ca(CH_3COO)_2 \cdot H_2O$ (Wako), and $Pb(CH_3COO)_2 \cdot 3H_2O$ (Wako) according to the procedure described in ref 11. The resulting solids were calcined at 773 K for 3 h after drying in air at 373 K overnight and are herein described as

[1]To whom correspondence should be addressed.

0022-4596/98 $25.00

"fresh catalysts." Particle sizes of 1.70–0.85 mm have been employed. The concentrations of Ca, Pb, and P were measured in an aqueous HNO_3 solution with inductively coupled plasma (ICP) spectrometry (SPS-1700, Seiko). The calcium and lead–calcium hydroxyapatites are denoted as HAp and Pb*xx*HAp, respectively, in which *xx* refers to 100Pb/[Pb + Ca] (atomic ratio). The BET surface area, apparent density, and the atomic ratios of Ca/P, Pb/P, and Pb/[Pb + Ca] are summarized in Table 1. A portion of each sample was further calcined at 873 or 973 K for 3 h in air to examine the thermal stability.

Apparatus and Procedure

The catalytic experiments were performed in a fixed-bed continuous-flow quartz reactor operated at atmospheric pressure. Details of the reactor design and catalyst packing procedure have been described elsewhere (41). Prior to reaction the catalyst was calcined *in situ* in an oxygen flow (25 ml/min) at a given temperature for 1 h. The typical reaction conditions were as follows: $W = 0.5$ g, $F = 30$ ml/min, $T = 973$ or 873 K, $P(CH_4) = 28.7$ kPa, $P(O_2) = 4.1$ kPa and $P(TCM) = 0$ or 0.17 kPa; balance to atmospheric pressure was provided by helium.

Analysis and Characterization

The reactants and products were analyzed with an on-stream gas chromatograph (Shimadzu GC-8APT) equipped with a TC detector and integrator (Shimadzu C-R6A). Additional analytical details and the procedure employed in the calculation of conversions and selectivities have been provided previously (41).

The surface areas of the catalysts were measured with a conventional BET nitrogen adsorption apparatus (Shibata P-700).

X-ray photoelectron spectroscopy (XPS; Shimadzu ESCA-1000AX) used monochromatized Mg$K\alpha$ radiation. The binding energies were corrected using 285 eV for C 1*s* as an internal standard. Argon-ion etching of the catalysts was carried out at 2 kV for 1 min with a sputtering rate estimated as 2 nm/min for SiO_2.

Powder X-ray diffraction (XRD) patterns were recorded with a Rigaku RINT 2500X diffractometer, using monochromatized Cu$K\alpha$ radiation. Patterns were recorded over the range $2\theta = 5$–60°.

Extended X-ray absorption fine structure (EXAFS) spectrometry near the Pb L_3 edge was performed (2.5 GeV) at the National Laboratory for High-Energy Physics with a storage ring current of ca. 320 mA. The X-rays were monochromatized with channel-cut Si(311) crystals and the absorption spectra were observed using ionization chambers in a transmission mode. The sample diluted with BN was compressed into a disk 13 mm in diameter. The photon energy was scanned in the range 12.5–14.1 keV for the Pb L_3 edge. Following the standard procedure, the EXAFS interference function $\chi(k)$ was extracted from the absorption spectra. The radial structure function $\phi(r)$ were obtained from the Fourier transforms of $k^3\chi(k)$. The backscattering amplitude and the phase shift function calculated by McKale *et al.* (50) were used. Fur the curve fitting, the range of interest for $\phi(r)$ was filtered with a Hamming window function and transformed back to k space, $\chi'(k)$. Curve-fitting calculations for $\chi'(k)$ (51) were performed over the k range of 3–8 Å.

RESULTS AND DISCUSSION

Properties of Catalysts

Figure 1 shows the XRD patterns of the fresh HAp and PbHAp catalysts. XRD patterns of HAp, Pb0.85HAp, and Pb7.5HAp were essentially identical and were identified as

TABLE 1
Surface Areas, Apparent Densities, and Compositions of Fresh Catalysts

	Catalyst					
	HAp	Pb0.85HAp	Pb5.7HAp	Pb12HAp	Pb20HAp	Pb35HAp
Area[a]	72.8	69.1	74.7	65.6	51.0	51.5
Density[b]	0.37	0.30	0.33	0.36	0.40	0.59
Ca/P[c]	1.65	1.76	1.58	1.66	1.36	0.98
	(1.55)	(1.53)	(1.43)	(1.35)	(1.19)	(1.05)
Pb/P[c]	0	0.02	0.10	0.23	0.34	0.53
	(0)	(0.03)	(0.09)	(0.17)	(0.34)	(0.47)
Pb/[Pb + Ca][c]	0	0.0085	0.057	0.12	0.20	0.35
	(0)	(0.018)	(0.062)	(0.11)	(0.22)	(0.31)

Note: Values in parentheses: atom ratios after additional calcination of the fresh catalysts at 973 K for 3 h in air.
[a]BET surface area (m^2/g).
[b]Apparent density (g/cm^3).
[c]Atomic ratio.

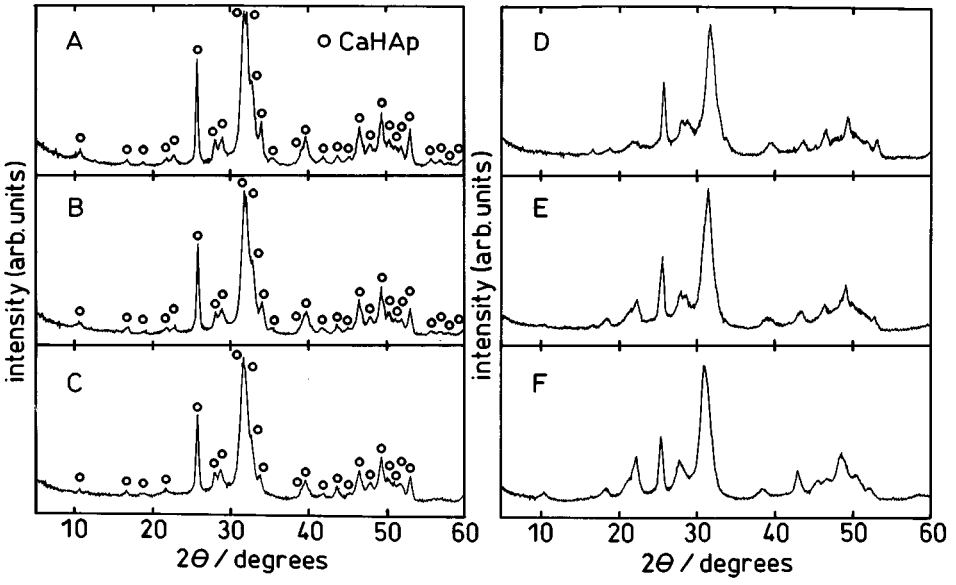

FIG. 1. XRD patterns of the fresh HAp and PbHAp catalysts. (A) HAp; (B) Pb0.85HAp; (C) Pb5.7HAp; (D) Pb12HAp; (E) Pb20HAp; (F) Pb35HAp. CaHAp: calcium hydroxyapatite.

$Ca_{10}(PO_4)_6(OH)_2$ [JCPDS 9-0432]. However, the remaining three XRD patterns were apparently different from those of calcium hydroxyapatite or $Pb_{10}(PO_4)_6(OH)_2$ [JCPDS 8-0259]. It is of interest to note the shift of the strongest peak in each catalyst with increasing lead in the catalysts. As shown in Table 2, the strongest peak moves monotonously to lower diffraction angle with increasing lead. Furthermore, the 2θ values for the strongest peak assigned to the (211) plane in PbHAp and $Ca_2Pb_8(PO_4)_6(OH)_2$ [JCPDS 40-1495] follow a trend similar to those for Pb12HAp, Pb20HAp, and Pb35HAp, indicating that the latter three possess the apatite structure, an observation reported previously by Bigi *et al.* (10, 11). Therefore the stoichiometry of the present catalysts is best represented as $Ca_{10-x}Pb_x(PO_4)_6(OH)_2$ $[0 \le x \le 3.5]$ rather than $(1-x)$ $Ca_{10}(PO_4)_6(OH)_2 + xPb(PO_4)_6(OH)_2$ $[0 \le x \le 0.35]$.

TABLE 2
Diffraction Angles for the Strongest XRD Peaks

Catalyst	Pb/[Pb + Ca]	2θ	Plane	Reference
$Ca_{10}(PO_4)_6(OH)_2$	0	31.772	(211)	JCPDS 9-0432
HAp	0	31.780	(211)	Present work
Pb0.85HAp	0.0085	31.700	(211)	Present work
Pb5.7HAp	0.057	31.690	(211)	Present work
Pb12HAp	0.12	31.660		Present work
Pb20HAp	0.20	31.460		Present work
Pb35HAp	0.35	30.920		Present work
$Ca_2Pb_8(PO_4)_6(OH)_2$	0.8	30.483	(211)	JCPDS 40-1495
$Pb_{10}(PO_4)_6(OH)_2$	1.0	30.114	(211)	JCPDS 8-0259

The effect of calcination of the samples at higher temperatures was investigated by additional heating at 873 and 973 K for 3 h in air. Although the samples subjected to the lower of these temperatures showed XRD patterns which were essentially identical to those found with the fresh samples, the use of the higher temperature evidently converted HAp, Pb0.85HAp, and Pb5.7HAp to calcium phosphate [JCPDS 9–0169] (Figs. 2A–C), while the XRD patterns for the more highly leaded samples also indicate the formation of the corresponding phosphate (Figs. 2D–F), in contrast to the usual observation that CaHAp is stable up to 1273 K (52). Although it is not uncommon for phosphate groups to be lost at high temperatures, no evidence for this was observed with the hydroxyapatites calcined at 973 K (Table 1). Additionally, calcium hydroxyapatites prepared from $Ca(NO_3)_2 \cdot 4H_2O$ and $(NH_4)_2HPO_4$ have been shown to be stable at 1048 K (41–43). Earlier work has shown that HAp retains the apatite structure after heating at 973 K (53). Others have found that both stoichiometric and nonstoichiometric HAp are stable at 1023 K (7). Although the presence of lead evidently has a negative influence on the thermal stability of the hydroxyapatites, the lead-free composition, as prepared for the present work, is also seen to have a reduced stability. It is tentatively concluded that the thermal stability of the apatites is dependent on both the nature of the cations and the procedures employed in their preparation. In view of the aforementioned, two temperatures, 973 and 873 K, have been employed for the reaction studies in the present work. At the higher temperature it was anticipated that the HAp would be converted to the corresponding phosphate while

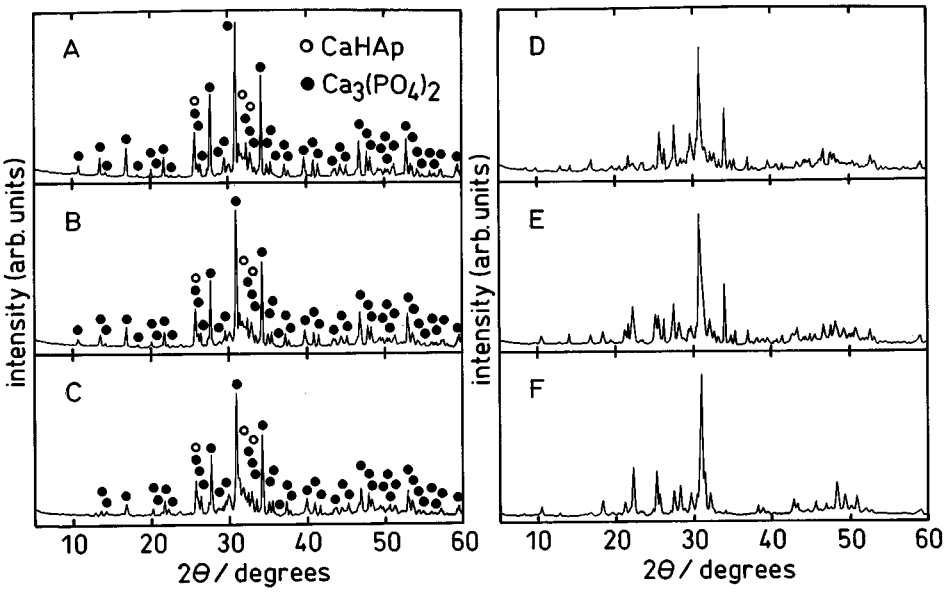

FIG. 2. XRD patterns of HAp and PbHAp calcined at 973 K for 3 h in air. Symbols: same as those in Fig. 1.

at the lower temperature the apatite structure should be retained.

Oxidation of Methane on HAp and PbHAp at 973 and 873 K

In the absence of TCM in the feedstream (Fig. 3A), the conversions of methane and oxygen increase with the first addition of lead but decrease on further increase of the lead content. However, for Pb12HAp and catalysts with higher lead contents, the conversions of methane and oxygen again increase. On addition of lead to HAp, the selectivity to C_{2+} hydrocarbons increases by a factor of approximately three and continues to increase, but more gradually, as the lead content increases. C_3 hydrocarbons appear in the product for Pb20.0HAp and Pb35.0HAp. While the selectivity to C_2H_4 increases with the first addition of lead, it remains approximately constant with further increases in the lead content. However, the selectivity to C_2H_6, while increasing on addition of lead, is higher for the Pb5.7HAp composition than any of the remaining catalysts. The selectivity to CO decreases continuously with addition of lead up to Pb20.0HAp. While it is clear that the addition of lead contributes directly to the enhancement of the selectivity to C_{2+} compounds and the reduction of that to carbon oxides, another factor appears to be operative in the process with lead-containing catalysts. With TCM in the feedstream, the conversion increases only marginally as the lead content is increased (Fig. 3B). While the selectivity to C_2H_4 remains relatively unchanged as lead is added, that to C_2H_6 increases, at least at shorter times-on-stream. Most noticeably, however, the carbon oxides in the product consist almost entirely of CO, with relatively small quantities of CH_3Cl being observed at the longer time-on-stream.

The XRD patterns of HAp, Pb0.85HAp, and Pb5.7HAp after use in the absence of TCM show that complete conversion to $Ca_3(PO_4)_2$ had occurred (Figs. 4A–C), and the remaining three catalysts also show evidence for the formation of the corresponding phosphates (Figs. 4D–F). After use in the oxidation reaction, but with TCM now present, the XRD patterns of the catalysts show little or no similarity to those of the hydroxyapatites or phosphates (Fig. 5). Since the catalysts such as HAp, Pb0.85HAp, and Pb5.7HAp containing the smaller lead contents have been converted to $Ca_{10}(PO_4)_6Cl_2$ (JCPDS 33-0271) as seen from the XRD patterns (Figs. 5A–C), and in the absence of reference XRD data for the chlorinated analogues for the remaining catalysts, the latter are assumed to have formed the corresponding chlorapatites. Since the catalysts are converted to the corresponding phosphate during the pretreatment at 973 K, these XRD results suggest that the phosphates are converted to the corresponding chlorapatite probably through the corresponding hydroxyapatite during the oxidation process when TCM is present. A similar conversion of the commercially available $Ca_3(PO_4)_2$ to $Ca_{10}(PO_4)_6Cl_2$ during the methane oxidation reaction on the phosphate when TCM is present in the feedstream has recently been reported (28).

Peaks attributed to Ca $2p_{1/2}$, Ca $2p_{3/2}$, O 1*s*, P 2*p*, Pb $4f_{5/2}$, and Pb $4f_{7/2}$ (when present) were detected at approximately 351, 348, 531.5, 133.5, 144, and 139 eV, respectively, in the XPS spectra of catalyst samples previously employed in obtaining the results reported in Fig. 3B, all of which were

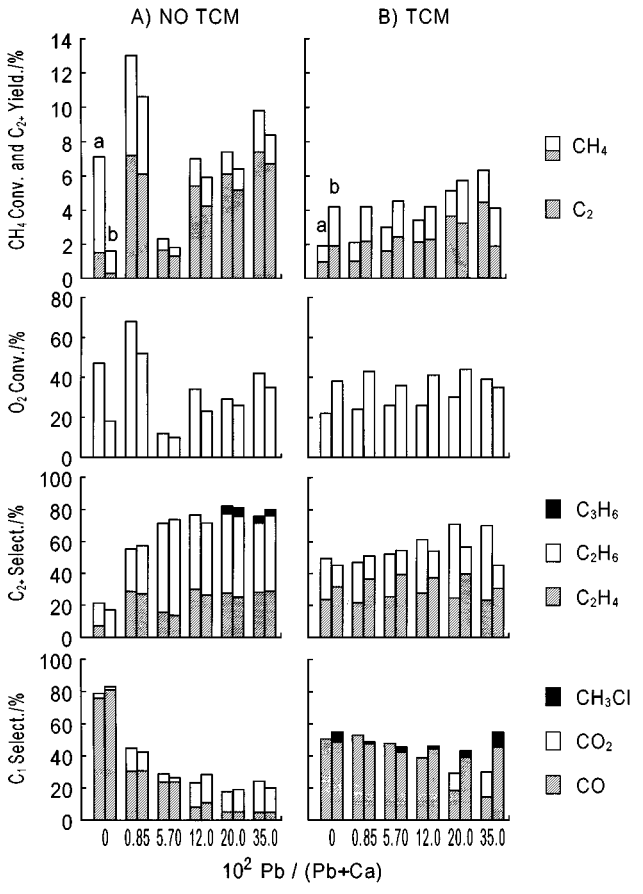

FIG. 3. Methane oxidation on HAp and PbHAp in the presence and absence of TCM at 973 K. Conditions: $W = 0.5$ g, $F = 30$ ml/min, $P(CH_4) = 28.7$ kPa, $P(O_2) = 4.1$ kPa, and $P(TCM) = 0.17$ kPa (when present) diluted with He. Catalysts were pretreated with O_2 (25 ml/min) at 973 K for 1 h. Symbols: (a) 0.5 h on-stream; (b) 6 h on-stream.

also found with each fresh catalyst, either before or after argon-ion etching. XPS spectra of catalysts which had been used in the oxidation process also contained a peak at approximately 199 eV due to Cl 2*p*. With some catalysts the peaks at approximately 142 and 137 eV for Pb $4f_{5/2}$ and $4f_{7/2}$, respectively, due to the metallic state of lead (Pb^0), were also detected.

Although the surface atomic ratios of Pb/P (Table 3) on the fresh catalysts as obtained from the XPS spectra are essentially identical to those in the bulk phase (Table 1), those of Ca/P show distinct differences. No systematic effects of the presence of TCM during the oxidation reaction could be detected in the surface atomic ratios of Ca/P and Pb/P but, not surprisingly, chlorine was detected on the surface of these catalysts although the Cl/P ratios are generally smaller than expected (0.33) for the stoichiometric chlorapatite (Table 3). Since the presence of a small quantity of phosphate was detected from the XRD patterns of the previously used (with TCM) catalysts, both the phosphates and chlorapatite apparently exist in the surface region.

The oxidation of methane was also examined at a pretreatment and reaction temperature of 873 K (Fig. 6). In the absence of TCM, maxima are observed in the conversions of methane and oxygen as well as the C_{2+} selectivity with increasing lead, in contrast with the results at 973 K, where a minimum was seen, while the selectivity to carbon oxides passes through a minimum (Fig. 6A). Following the oxidation at 873 K without TCM, significant quantities of the hydroxyapatites as well as the corresponding phosphates were found to be present (Fig. 7). Evidently the conversion of methane is strongly influenced by the structure of the catalysts while the selectivities are more strongly dependent upon the lead content.

With TCM present in the feedstream, the patterns observed in its absence remain, although the conversions are depressed (Figs. 6B and 8). Selectivities to C_{2+} hydrocarbons remain relatively unchanged while the selectivity to CO is, as observed at 973 K, increased. However, the effect of time-on-stream is particularly evident at the lower temperature with selectivities to CO_2 which, although significant at the lower time-on-stream, have vanished at the longer time-on-stream. Again, methyl chloride is observed at the longer time-on-stream with significantly higher selectivities than observed at 973 K. Similar time-on-stream effects on the selectivities to CO and CO_2 in the presence of TCM have been reported for calcium (41–43) and strontium (45, 46) hydroxyapatites, providing evidence for the interaction of TCM with the surface to form chlorapatite and the cumulative effect of its formation on the oxidation reaction.

Although some deactivation is evidently occurring with the catalysts employed in the absence of TCM, particularly where lead is not present, the decrease in conversion with time-on-stream for the lead-containing catalysts is relatively small at either reaction temperature. With TCM present, the conversion increases with time-on-stream at the higher reaction temperature, while extensive deactivation, as judged by decreases in the conversion, occurs at the lower reaction temperature.

The XPS spectra of the catalysts previously employed with TCM in the oxidation at 873 K contained the peaks found with the catalysts after use at 973 K. Metallic lead was in evidence in the used catalysts, particularly those subjected to the lower reaction temperature (Table 3), implying that Pb^{2+} cations in the hydroxyapatites are reduced, but not those in the phosphates. No systematic effects on the values of Ca/P or Pb/P were observed as a result of the introduction of TCM but the values for Cl/P were generally larger after use of the catalysts at 873 K. Although care must be taken in any deductions of trends in the Cl/P ratios, it is tempting to conclude that the values found with the catalysts used at 873 K pass through a minimum with lead content while those at 973 K display

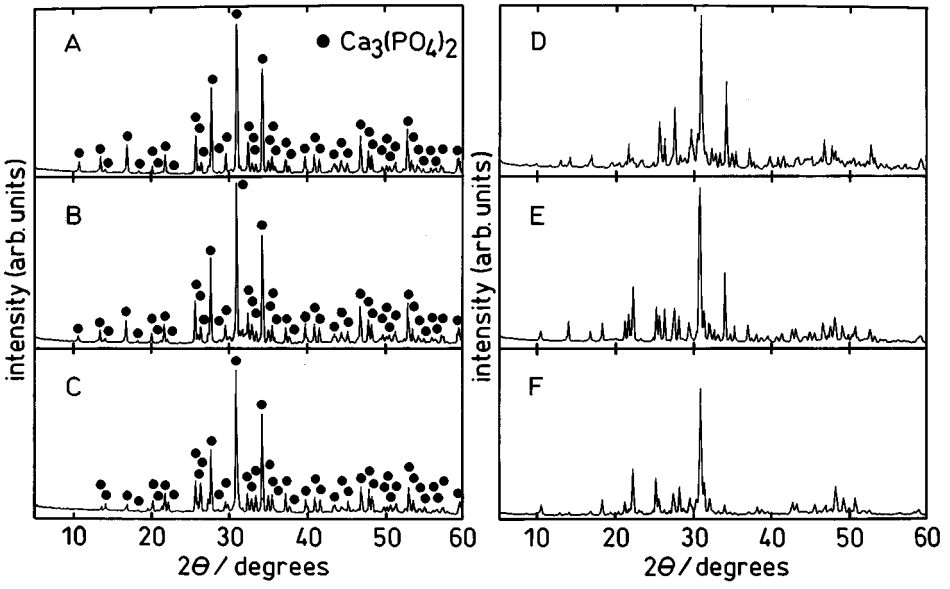

FIG. 4. XRD patterns of catalysts previously employed in obtaining the results shown in Fig. 3A. Symbols: same as those in Fig. 1.

a maximum. Further, the minimum and maximum Cl/P values closely approximate those expected for the chlorapatite. Such behavior appears to reflect, reciprocally, the conversion of methane at these two temperatures. Tentatively, it may be concluded that both deficits and excesses in the stoichiometry as related to that of chlorapatite are disadvantageous to the conversion of methane.

Structural Properties

While not precluding the participation of others, oxygen species have frequently been postulated as the active sites in the methane oxidation process. The aforementioned results demonstrate that cations of Pb play a role in the oxidation process, although the nature of this participation is unclear.

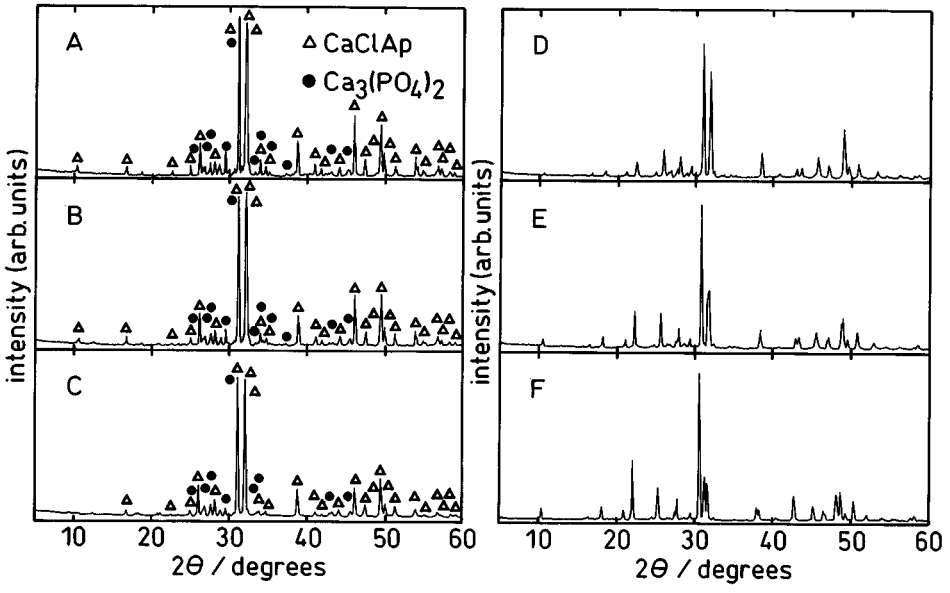

FIG. 5. XRD patterns of catalysts previously employed in obtaining the results shown in Fig. 3B. Symbols: same as those in Fig. 1.

TABLE 3
XPS Results of Catalysts Fresh and after Use[a] in the Presence of TCM

		Ca/P[c]			Pb/P[c]			Cl/P[c]		
Catalyst	T^b	F[d]	873[e]	973[e]	F[d]	873[e]	973[e]	F[d]	873[e]	973[e]
HAp	0	1.15	1.16	1.21					0.45	0.30
	1	1.24	1.06	1.33					0.28	0.23
Pb0.85HAp	0	1.15	1.28	1.19	0.01	0.01	0.006		0.60	0.22
	1	1.31	1.25	1.36	0.004	0.008	0.008		0.45	0.20
Pb5.7HAp	0	1.08	1.09	1.20	0.08	0.09	0.04		0.32	0.23
	1	1.47	1.76	1.45	0.03	0.04	0.02		0.33	0.23
					(—	0.2	—)[f]			
Pb12HAp	0	0.96	1.11	1.19	0.19	0.22	0.23		0.32	0.32
	1	1.73	1.74	1.91	0.10	0.15	0.13		0.33	0.32
					(—	0.3	0.1)[f]			
Pb20HAp	0	1.01	1.01	0.98	0.37	0.42	0.24		0.44	0.20
	1	1.86	1.88	1.63	0.23	0.37	0.21		0.48	0.24
					(0.3	0.3	0.2)[f]			
Pb35HAp	0	1.00	0.69	0.69	0.65	0.55	0.35		0.39	0.19
	1	1.70	1.55	1.40	0.51	0.61	0.42		0.38	0.24
					(0.3	0.2	0.2)[f]			

[a]Previously employed in obtaining the results reported in Figs. 3B and 6B, but after 6 h on-stream.
[b]Etching time (min).
[c]Atomic ratio.
[d]Fresh catalyst.
[e]Reaction and pretreatment temperatures (K).
[f]Atomic ratio of Pb^0/Pb^{2+}.

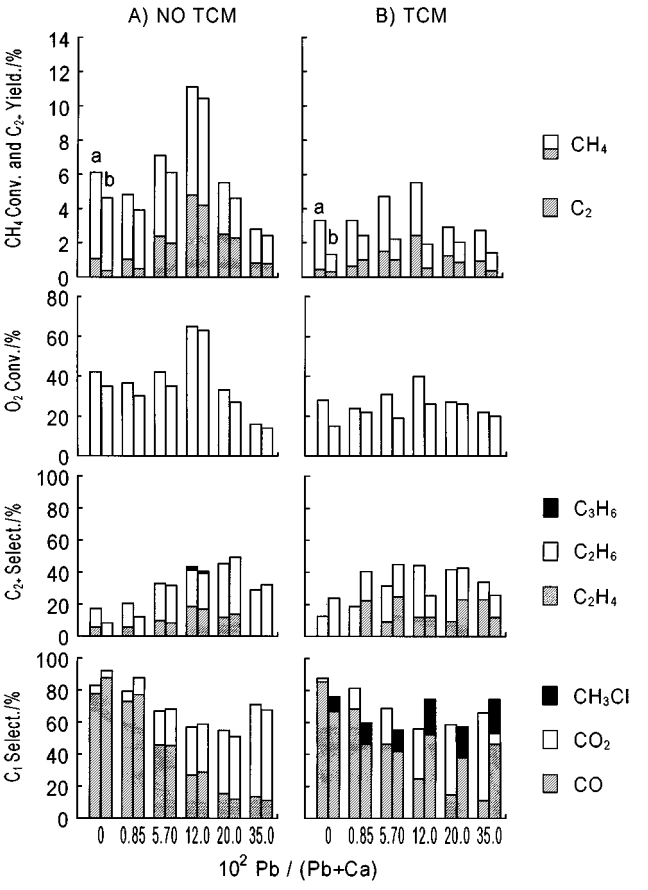

FIG. 6. Methane oxidation on HAp and PbHAp in the presence and absence of TCM at 873 K. Conditions and symbols: same as those in Fig. 3 except pretreatment and reaction temperatures (both 873 K).

It is not unreasonable to suggest that it is most probable that the role of lead in methane activation is indirect in the sense of perturbations on the oxygen species of the catalysts. Although EXAFS analyses provide only bulk phase information, nevertheless such data can provide semiquantitative evidence of any surface structural influences resulting from the addition of lead. Recent work has shown that correlations exist between the catalytic properties of strontium–lead (49) hydroxyapatite and nearest-neighbor bond distances as estimated from EXAFS data. The X-ray absorption near-edge structure (XANES) spectra near the Pb L_3 edge are shown in Fig. 9. The shape of the XANES spectra and the edge position of the PbHAp catalysts near the Pb L_3 edge were similar, indicating that the electronic configuration and site symmetry of the lead in each sample are not significantly different. The Fourier transforms of the EXAFS oscillation around the Pb L_3 edge of the PbHAp catalysts are shown in Fig. 10. Phase shifts are not corrected in these spectra. The strongest peak in each spectrum corresponds to the nearest-neighbor Pb–O distance (54). Since the data obtained at the nearest-neighbor distances, are more precise than those for other distances the reliability of the phase shift and amplitude functions is tested at approximately the nearest distance by fitting the observed EXAFS of each fresh catalyst. Optimum curve fitting around the Pb L_3 edge of the fresh leaded catalysts is shown in Fig. 11 and the results of these analyses are summarized in Table 4. Although the estimated deviations should be noted, the nearest-neighbor distances of the Pb–O bonds follow the order Pb0.85HAp > Pb5.7HAp > Pb12HAp = Pb20HAp > Pb35HAp, indicative of a more highly packed environment of the oxygen as the lead content increases. The selectivity to C_{2+} hydrocarbons where TCM is absent, particularly at 873 K, at which temperature the apatite structure is prevalent during the oxidation, is seen to increase as the Pb–O distance decreases (Figs. 3A and 6A) while comcomitantly the selectivity to total carbon oxides decreases. Since the nearest Pb–O distances show no correlation with the conversion of methane, such structural parameters appear to be related to processes which are subsequent to the activation of methane. The suppression of secondary oxidation processes, such as those which lead to higher and lower selectivities to CO_x and C_{2+} hydrocarbons, respectively, may be dependent as much, if not more, on the ability of surface Pb to stabilize the methyl radicals in

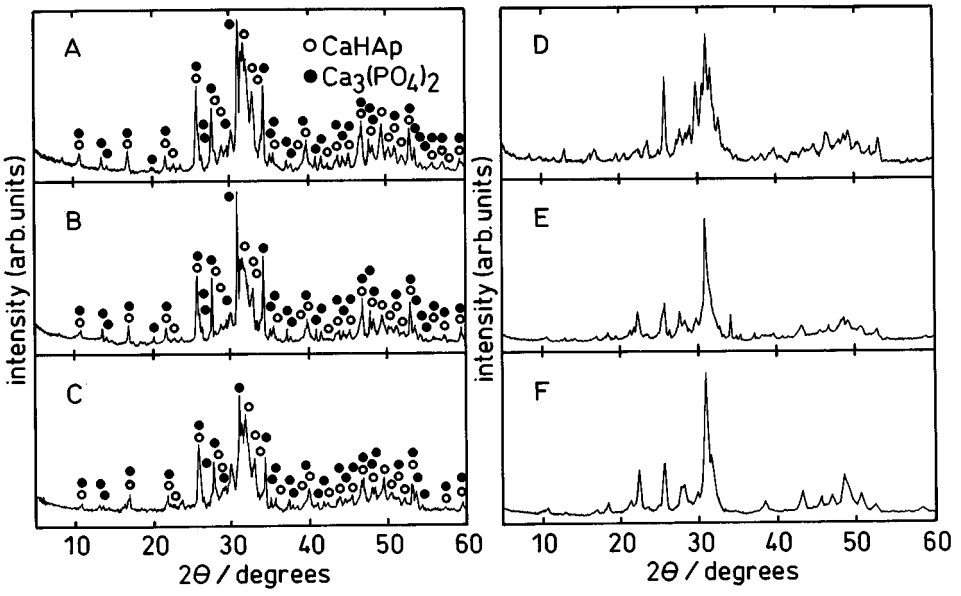

FIG. 7. XRD patterns of catalysts previously employed in obtaining the results shown in Fig. 6A. Symbols: same as those in Fig. 1.

close proximity to each other than on the electronic density perturbation induced in the surface oxygen species.

CONCLUSIONS

1. Calcium hydroxyapatite, with and without added lead, as prepared from lead and/or calcium acetate with sodium phosphate, was stable at 873 K but converted to the corresponding phosphate at 973 K.

2. In the absence of TCM in the methane oxidation feedstream on HAp and PbHAp, the conversion of methane and oxygen at 973 K showed concave patterns with increasing lead in the catalysts consisting of the corresponding phosphates formed during the pretreatment while convex

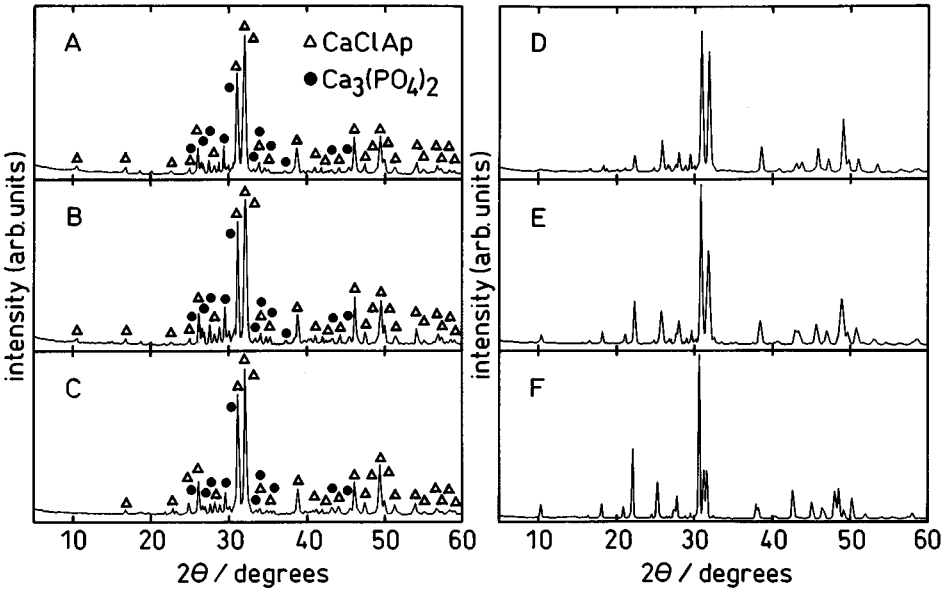

FIG. 8. XRD patterns of catalysts previously employed in obtaining the results shown in Fig. 6B. Symbols: same as those in Fig. 1.

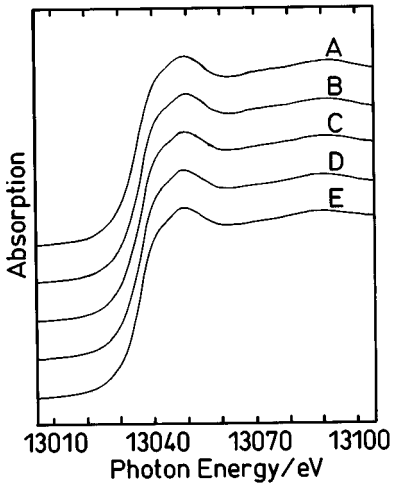

FIG. 9. XANES spectra of fresh PbHAp catalysts: (A) Pb0.85HAp; (B) Pb5.7HAp; (C) Pb12HAp; (D) Pb20HAp; (E) Pb35HAp.

patterns were observed at 873 K, at which temperature the hydroxyapatite structure is intact.

3. The selectivities to C_1 and C_{2+} compounds decreased and increased, respectively, with increasing lead content of the catalysts at 873 and 973 K.

4. Although the conversion and selectivity were relatively insensitive to the lead content in the presence of TCM at 973 K, the formation of methyl chloride and the depression of the deep oxidation to carbon dioxide were evident, particularly at the longer time-on-stream.

5. At 873 K in the presence of TCM, the convex patterns of the conversion and the effects of the lead content in the catalysts on the total selectivities to C_1 and C_{2+} compounds were similar to those observed in the absence of TCM but the conversions decreased on addition of TCM and increasing time-on-stream. The formation of methyl chloride and

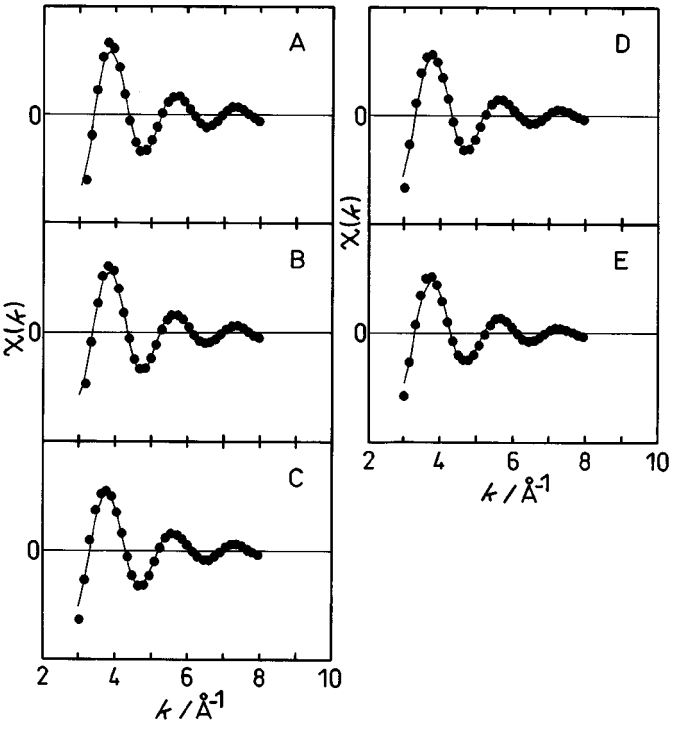

FIG. 11. Curve fitting of fresh PbHAp. Symbols: solid line, experimental data; closed circles, calculated values. Other symbols: same as those in Fig. 9.

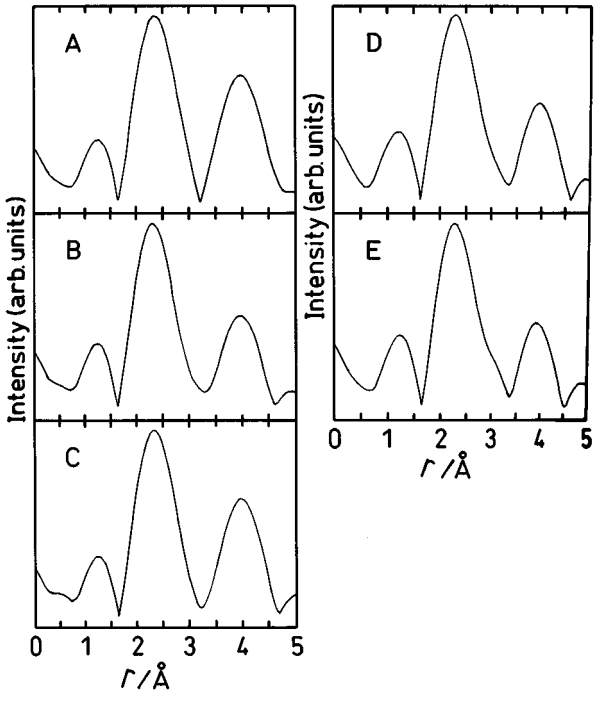

FIG. 10. Fourier transformation of k^3-weighted EXAFS oscillation near the Pb L_3 edge of fresh PbHap catalysts. Symbols: same as those in Fig. 9.

TABLE 4
Results of Curve-Fitting Analyses for Fresh Catalysts

Catalyst	r_{Pb-O}[a] (Å)	N[b]	σ[c] (Å)	E_0 (eV)	R[d] (%)
Pb0.85HAp	2.36	3.5	0.120	0.52	20.4
Pb5.7HAp	2.35	3.8	0.124	−0.42	17.0
Pb12HAp	2.34	4.0	0.128	−2.24	17.5
Pb20HAp	2.34	4.2	0.135	−2.24	19.5
Pb35HAp	2.33	4.3	0.137	−2.63	20.0

[a]Distance; estimated maximum deviation (±0.01).
[b]Coordination number; estimated maximum deviation (± 1).
[c]Debye–Waller (like) factor.
[d]Reliability factor.

the depression of the deep oxidation to carbon dioxide were again observed in the presence of TCM.

6. The selectivity to C_{2+} hydrocarbons at 873 and 973 K in the absence of TCM increases with decreasing nearest-neighbour Pb–O distances in the lead-containing catalyts.

ACKNOWLEDGMENTS

This work was partially funded by a Grant for Natural Gas Research from The Japan Petroleum Institute to S.S. and the Natural Sciences and Engineering Research Council of Canada to J.B.M. and has been performed under the approval of the Photon Factory Program Advisory Committee (Proposal 95G193).

REFERENCES

1. J. A. S. Bett, L. G. Christner, and W. K. Hall, *J. Catal.* **13,** 332 (1969).
2. C. L. Kibby and W. K. Hall, *J. Catal.* **29,** 144 (1993).
3. C. L. Kibby and W. K. Hall, *J. Catal.* **31,** 65 (1973).
4. H. Monma, *J. Catal.* **75,** 200 (1982).
5. Y. Imizu, M. Kadoya, and H. Abe, *Chem. Lett*. 415 (1982).
6. Y. Izumi, S. Sato, and K. Urabe, *Chem. Lett*. 1649 (1983).
7. J. A. Bett, L. G. Christner, and W. K. Hall, *J. Am. Chem. Soc*. **89,** 5535 (1967).
8. T. Suzuki, T. Hatsushika, and Y. Hayakawa, *J. Chem. Soc*., *Faraday Trans. 1* **77,** 1059 (1981).
9. T. Suzuki, T. Hatsushika, and M. Miyake, *J. Chem. Soc*., *Faraday Trans. 1* **78,** 3605 (1982).
10. A. Bigi, M. Ripamonti, S. Bruckner, M. Gazzano, N. Roveri, and S. A. Thomas, *Acta Crystallogr*., *B* **45,** 247 (1991).
11. A. Bigi, M. Gandolfi, M. Gazzano, A. Ripamonti, N. Roveri, and S. A. Thomas, *J. Chem. Soc*., *Dalton Trans.* 2883 (1991).
12. W. Hinsen, W. Bytyn, and M. Baerns, *in* "Proceedings of the 8th International Congress on Catalysis, Berlin, 1984," Vol. 3, p. 581. Verlag Chemie, Weinheim, 1984.
13. K. Otsuka, K. Jinno, and A. Morikawa, *Chem. Lett*. 499 (1985).
14. M. Y. Sinev, G. A. Vorob'eva, and U. N. Kornak, *Kinet. Katal.* **27,** 1007 (1986).
15. W. Bytyn and M. Baerns, *Appl. Catal.* **28,** 199 (1986).
16. J. A. S. P. Carreiro and M. Baerns, *React. Kinet. Catal. Lett*. **35,** 49 (1987).
17. K. Asami, S. Hashimoto, T. Shikada, K. Fujimoto, and H. Tominaga, *Ind. Eng. Chem. Res.* **26,** 1485 (1987).
18. J. A. Roos, A. G. Bakker, H. Bosch, J. C. van Ommen, and J. R. H. Ross, *Catal. Today* **1,** 133 (1987).
19. K. Asami, T. Shikada, K. Fujimoto, and H. Tominaga, *Ind. Eng. Chem. Res.* **26,** 2348 (1987).
20. J. A. S. P. Carreiro, G. Follmer, L. Lehman, and M. Baerns, *in* "Proceedings of the 9th International Congress on Catalysis, Calgary, 1988" (M. J. Phillips and M. Ternan, Eds.), Vol. 2, p. 891. Chemical Institute of Canada, Ottawa, 1988.
21. K. Aika and T. Nishiyama, *in* "Proceedings of the 9th International Congress on Catalysis, Calgary, 1988" (M. J. Phillips and M. Ternan, Eds.), Vol. 2, p. 907. Chemical Institute of Canada, Ottawa, 1988.
22. J. P. Bartek, J. M. Hupp, J. F. Brazdil, and R. K. Grasselli, *Catal. Today* **3,** 117 (1988).
23. J. M. Thomas, W. Ueda, J. Williams, and K. D. M. Harris, *Faraday Discuss*., *Chem. Soc*. **87,** 33 (1989).
24. K. C. C. Kharas and J. H. Lunsford, *J. Am. Chem. Soc*. **111,** 2336 (1989).
25. K. Fujimoto, S. Hashimoto, K. Asami, K. Omata, and H. Tominaga, *Appl. Catal*. **50,** 223 (1989).
26. S. K. Agarwal, R. A. Migone, and G. Marcelin, *J. Catal.* **121,** 110 (1990).
27. S. K. Agarwal, R. A. Migone, and G. Marcelin, *J. Catal.* **123,** 228 (1990).
28. M. Y. Sinev, V. Y. Bychkov, V. N. Korchak, and O. V. Krilov, *Catal. Today* **6,** 543 (1990).
29. T. Grzybek and M. Baerns, *J. Catal.* **129,** 106 (1991).
30. K. Aika, N. Fujimoto, M. Kobayashi, and E. Iwamatsu, *J. Catal*. **127,** 1 (1991).
31. K. J. Smith, T. M. Painter, and J. Galuszka, *Catal. Lett*. **11,** 301 (1991).
32. S.-E. Park and J.-S. Chang, *Appl. Catal. A* **85,** 117 (1992).
33. T. Ohno and J. B. Moffat, *Catal. Lett*. **16,** 181 (1992).
34. R. Mariscal, J. Soria, M. A. Pena, and J. L. G. Fierro, *Appl. Catal. A*. **111,** 79 (1994).
35. J.-S. Chang and S.-E. Park, *Bull. Korean Chem. Soc*. **16,** 1148 (1995).
36. Y. Matsumura, J. B. Moffat, S. Sugiyama, H. Hayashi, N. Shigemoto, and K. Saitoh, *J. Chem. Soc*., *Faraday Trans.* **90,** 2133 (1994).
37. Y. Matsumura, S. Sugiyama, H. Hayashi, and J. B. Moffat, *J. Solid State Chem.* **114,** 138 (1995).
38. Y. Matsumura, S. Sugiyama, H. Hayashi, and J. B. Moffat, *Catal. Lett*. **30,** 235 (1995).
39. Y. Matsumura and J. B. Moffat, *Catal. Lett*. **17,** 197 (1993).
40. Y. Matsumura and J. B. Moffat, *J. Catal.* **148,** 323 (1994).
41. S. Sugiyama, T. Minami, H. Hayashi, M. Tanaka, N. Shigemoto, and J. B. Moffat, *J. Chem. Soc*., *Faraday Trans.* **92,** 293 (1996).
42. S. Sugiyama, T. Minami, T. Moriga, H. Hayashi, K. Koto, M. Tanaka, and J. B. Moffat, *J. Mater. Chem.* **6,** 459 (1996).
43. S. Sugiyama, T. Minami, H. Hayashi, M. Tanaka, N. Shigemoto, and J. B. Moffat, *Energy and Fuels* **10,** 828 (1996).
44. Y. Matsumura, S. Sugiyama, H. Hayashi, N. Shigemoto, K. Saitoh, and J. B. Moffat, *J. Mol. Catal.* **92,** 81 (1994).
45. S. Sugiyama, T. Minami, H. Hayashi, M. Tanaka, and J. B. Moffat, *J. Solid State Chem.* **126,** 242 (1996).
46. S. Sugiyama, T. Minami, T. Higaki, H. Hayashi, and J. B. Moffat, *Ind. Eng. Chem. Res.* **36,** 328 (1997).
47. J. B. Moffat, S. Sugiyama, and H. Hayashi, *Catal. Today* **109,** 1 (1997). [and references therein].
48. S. Sugiyama, Y. Iguchi, T. Minami, H. Hayashi, and J. B. Moffat, *Catal. Lett*. **46,** 279 (1997).
49. S. Sugiyama, Y. Iguchi, H. Nishioka, T. Minami, T. Moriga, H. Hayashi, and J. B. Moffat, *J. Catal.* [submitted]
50. A. G. McKale, B. W. Veal, A. P. Paulikas, S. K. Chan, and G. S. Knapp, *J. Am. Chem. Soc*. **110,** 3763 (1988).
51. H. Sakane, T. Miyanaga, I. Watanabe, N. Matsubayashi, S. Ikeda, and Y. Yokoyama, *Jpn. J. Appl. Phys*., *Part 1* **32,** 4641 (1993).
52. D. E. C. Corbridge, "The Structural Chemistry of Phosphorus," p. 90 Elsevier, Amsterdam, 1974.
53. H. Monma, S. Ueno, and T. Kanazawa, *J. Chem. Tech. Biotechnol*. **31,** 15 (1981).
54. S. Sugiyama, T. Moriga, M. Goda, H. Hayashi, and J. B. Moffat, *J. Chem. Soc*., *Faraday Trans.* **92,** 4305 (1996).